RSC Advances

RSC Advances

www.rsc.org/advances

ROYAL SOCIETY OF CHEMISTRY

www.rsc.org/advances
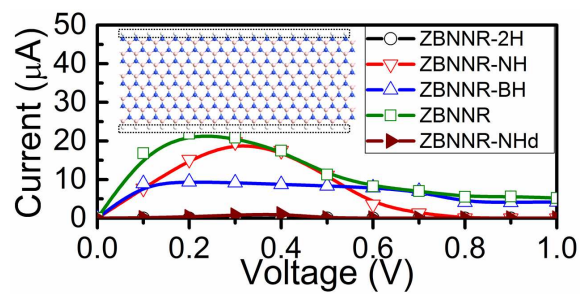
The zigzag boron nitride nanoribbons (ZBNNRs) based devices exhibit the intrinsic negative differential resistance (NDR) characteristics.

RSC Advances

ARTICLE

Intrinsic Negative Differential Resistance Characteristics in Zigzag Boron Nitride Nanoribbons

Yipeng An,*[a] Kedong Wang,[a] Guangrui Jia,[a] Tianxing Wang,[a] Zhaoyong Jiao,[a] Zhaoming Fu,[a] Xingli Chu,[a] Guoliang Xu[a] and Chuanlu Yang[b]

We investigate the charge transport properties of the zigzag boron nitride nanoribbons (ZBNNRs) with various hydrogen passivations employing the density functional theory (DFT) combined with the non-equilibrium Green's function (NEGF) formalism. The calculated results reveal that the ZBNNR-based devices exhibit the negative differential resistance (NDR) characteristics except those models whose both edges are passivated, due to the mechanism that the overlaps of bands near the Fermi level between the left and right electrodes get smaller or disappear under a high bias. The NDR characteristics of the perfect ZBNNRs with one or two bare edges are weakly dependent on their widths. It is one intrinsic NDR characteristic of the ZBNNR-based devices, including some defective structures. The intuitive electronic current channels are plotted and analyzed to better understand the charge transport mechanisms. Our results suggest that the ZBNNR-based structures could be the favorable candidates for preparing the nanoscale NDR devices.

1 Introduction

Single-layer materials could exhibit some novel physical phenomena and potential applications in nanoscale electronics.[1-17] Graphene, single atomic layers of carbon, has attracted extensive research interest over the past decades since its successful fabrication in 2004,[2,3] due to its special electronic structures and fantastic electronic transport behaviors.[4-6] If terminated in one direction, these single-layer materials can be further fabricated into a new kind of quasia-one-dimensional structure called nanoribbons. Several prototype devices based on graphene nanoribbons (GNRs), including field-effect transistors (FETs)[7] and devices exhibiting negative differential resistance (NDR),[8,9] have been theoretically predicated and experimentally fabricated.[10,11]

Hexagonal boron nitride (h-BN) single layer, the III-V analogue of graphene, has also attained much attention due to its super thermal and chemical stabilities.[12-32] Two-dimensional (2D) h-BN sheet exhibits a direct energy gap of 4.78 eV,[12] dramatically different from graphene which is a gapless semiconductor. Several groups have successively prepared the 2D boron nitride nanostructures.[13-17] The purity is gradually improved and the cost is also decreasing.[16,17] BN nanoribbons (BNNRs), mostly terminated with zigzag edges, has been successfully fabricated via boron nitride nanotube unwrapping since 2010.[14,15] Some groups have theoretically investigated the electronic structures of the single layer BNNRs by considering different edge decorations,[18] sample sizes,[19] defects,[20,21] doping,[22] and external fields,[23-26] etc. However, it needs to pay more attentions to the charge transport properties of BNNRs.

Especially, it is one interesting topic to know how the edge decorations and ribbon widths affect their charge transport and applications in nanoscale electronics.

In this paper, we investigate the charge transport properties of zigzag BNNRs (ZBNNRs) by first-principles calculations within the local density approximation (LDA), and predict the intrinsic negative differential resistance characteristics in ZBNNRs with bare B edge, bare N edge, as well as bare B and N edges. The ZBNNRs with both edges passivated by hydrogen exhibit the wide gap semiconductor properties, and do not conduct electricity under finite bias voltages. However, the ZNNRs with one or two bare edges show the metallic or half-metallic characteristics, and their current–voltage (I–V) curves all present the NDR behaviors rather than the linear characteristics. The current through the ZBNNRs with bare B edge belongs to the B→B hop current, which flows mainly along the bare B edge. However, for the ZBNNRs with bare N edge, there exist three current channels, i.e., N→B bond current, as well as B→N and N→N hop current channels under a low bias, but only N→B bond current channel under a high bias. All these current channels are along or close to the bare N edge. What's more, for the ZBNNRs with bare B and N edges, there exist four current channels under a low bias. There is one additional B→B hop current channel along the bare B edge, except that another three are same to the case of the ZBNNRs with bare N edge. While, only one N→B bond current channel is available under a high bias. Interestingly, the results also reveal that the NDR characteristic of the ZBNNRs is independent of ribbon widths, and survives in the defective ZBNNRs with certain boron or nitrogen atom

vacancy defect. Unlike the graphene nanoribbons, which can present the NDR phenomena by defecting,[9] doping,[32] etc., it is the intrinsic characteristic for the ZBNNRs. Therefore, we propose that the ZBNNRs could be the favorable potential materials for NDR nanodevices.

2 Models and method

The two-probe ZBNNR models we study are illustrated in Fig. 1(a). Here, the ZBNNRs are labeled by the number of parallel zigzag chains, which defines the ribbon width. The ZBNNRs with n B-N chains is, thus, named as n-ZBNNR. In terms of hydrogen passivation of the edge, the ZBNNRs are divided into four subgroups: (1) both edges are passivated (labeled as n-ZBNNR-2H), (2) only the N edge is passivated (labeled as n-ZBNNR-NH), (3) only the B edge is passivated (labeled as n-ZBNNR-BH), and (4) no edge is passivated (labeled as n-ZBNNR). Such two-probe system is divided into three regions: the left electrode (L), the right electrode (R), and the central scattering region (C). Each electrode is described by a supercell with three repeated unit cells along the transport direction.

The first-principles calculations of the charge transport properties of the ZBNNRs (with various hydrogen passivations at the edges) were performed by using the density functional theory (DFT) with the LDA combined with the non-equilibrium Green's function (NEGF) formalism as implemented in the ATK code.[33-35] In the calculations, the geometry structure of each two-probe system was first relaxed until the absolute value of force acting on each atom is less than 0.05 eV/Å^{-1} under the periodic boundary condition. The core electrons of all atoms were described by the Norm-conserving Troullier–Martins pseudopotentials,[36] while the valence electrons were described by a double-ζ plus polarization (DZP) basis set. The Monkhorst–Pack k-points grid $1\times1\times100$ was used to sample the Brillouin zone of the electrodes, and the real-space grid techniques were used with the energy cutoff of 100 Ry as a required cutoff energy in numerical integrations and the solution of Poisson equation using fast Fourier transform (FFT). We allow for an external bias V_b ($V_b = V_L - V_R$, and $V_{L/R}$ is the bias voltage applied on the left (L)/right (R) electrode) to be applied between the two electrodes. The applied bias thus shifts all energies in the left electrode, and a positive bias gives rise to an electric current from the left to the right electrode. The current I through these ZBNNR based devices can be calculated from the Landauer–Büttiker formula[37]

$$I(V_b) = \frac{2e}{h} \int_{-\infty}^{\infty} T(E, V_b)[f_L(E - \mu_L) - f_R(E - \mu_R)]dE$$

where $T(E, V_b)$ is the bias-dependent transmission coefficient calculated from the Green's functions, and $f_{L/R}$ is the Fermi-Dirac distribution function of the left (L)/right (R) electrode. More details of the calculation method can be found in previous reports.[33-35]
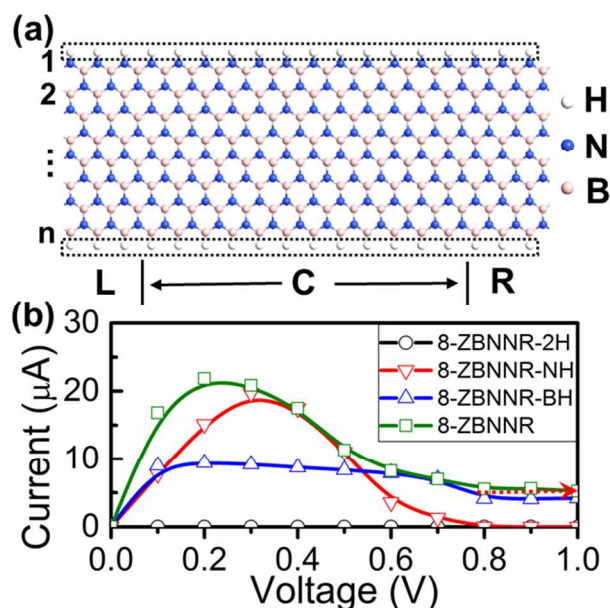
Fig. 1 (a) The geometric structures of ZBNNR-based devices with various hydrogen passivations at the edges: n-ZBNNR-2H, n-ZBNNR-NH, n-ZBNNR-BH, and n-ZBNNR. (b) Calculated I–V curves of 8-ZBNNR-based devices.

3 Results and discussion

We first investigate the charge transport properties of the 8-ZBNNRs with various hydrogen passivations at the edges. The calculated I–V curves are depicted in Fig. 1(b). As can be seen, the current through 8-ZBNNR-2H is zero, due to its semiconductor characteristic.[18] However, all the I–V curves of 8-ZBNNR-NH, 8-ZBNNR-BH, and 8-ZBNNR exhibit NDR behaviors. For instance, the current through 8-ZBNNBR-NH reaches to a maximum at the bias of 0.3 V and then drops down, until to zero under a threshold voltage of 0.8 V. Differently, the current through 8-ZBNNR-BN and 8-ZBNNR reaches up to the peak at 0.2 V and then drops down to one non-zero steady value, respectively. The current through 8-ZBNNR is the greatest value under the finite biases, while it is larger for 8-ZBNNR-NH than that of 8-ZBNNR-BH under a low bias but the relationship reverses under a high bias (i.e., beyond 0.5 V bias).

Here, we employ the band structure to understand the NDR behaviors of the 8-ZBNNR-based devices. Generally, the distinct charge transport properties should arise from the characteristics of band structures of the ZBNNRs with various hydrogen passivations, as shown in Fig. 2. The 8-ZBNNR-2H is the semiconductor with a gap of 3.85 eV, consistent with the previously published result.[18] For the 8-ZBNNR-NH, it exhibits metallic feature, and there is one band crossing the Fermi level (E_F), as shown in Fig. 2(b). The band is ascribed to the σ-dangling bond states at the edge B atoms (labeled as B_σ), which is mainly composed of a p_y orbital of edge B atoms according to the wave function at Γ point. For the case of 8-ZBNNR-BH, it exhibits half-metallic feature, as shown in Fig. 2(c). There are two bands crossing the E_F level, which can be identified as the σ-dangling bond states at the edge N atoms (labeled as N_σ, composed of N p_y orbital) and the π states at the N atoms close to the bare N edge (labeled as N_π, composed of N p_x orbital) according to the wave functions, respectively. Fig. 2(d) shows the band structure of the 8-ZBNNR which also presents

metallic feature, consistent with the previous ab initio calculations.[12] There are three bands crossing the E_F level, which originates from the σ-dangling bond states at the edge N and B atoms, as well as the π states at the N atoms close to the bare N edge, respectively.
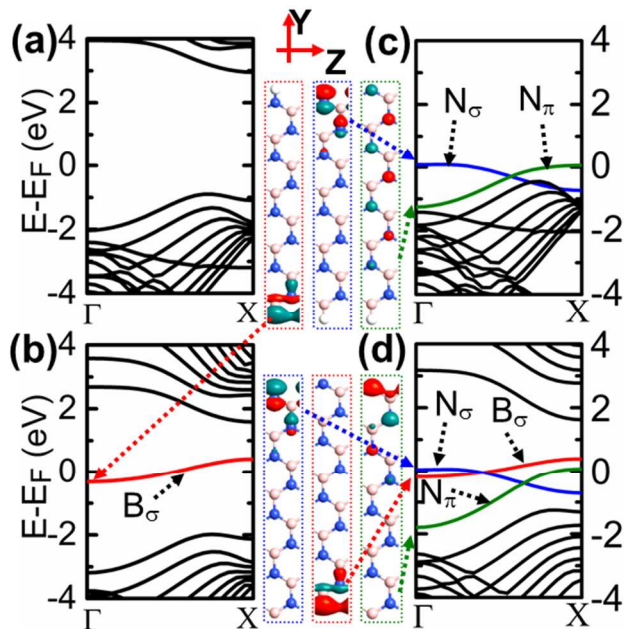
Fig. 2 Band structure and wave functions of the (a) 8-ZBNNR-2H, (b) 8-ZBNNR-NH, (c) 8-BNNR-BH, and (d) 8-ZBNNR. The Fermi level is set at zero.

For the semiconductor 8-ZBNNR-2H, the electrons are obviously forbidden to propagate through the nanojunction due to the wide band gap (shown in Fig. 2(a)), leading to zero current under the finite applied bias voltages, as shown in Fig. 1(b). Unlike the zigzag (ZGNRs) with *odd*-numbered chain which shows the linear trend,[38] the *I–V* curve of 8-ZBNNR-NH exhibits an interesting NDR behavior. To understand this NDR phenomenon, we give the bias-dependent transmission spectra and band structures of both left and right electrodes for the 8-ZBNNR-NH in Fig. 3, which is the most intuitive representation of electronic structures and charge transport properties of a two-probe device. Under the positive bias, the energy bands shift downward and upward for the left and right electrodes, respectively. At the bias of 0.3 V, the $B_σ$ band of left electrode has the largest overlapping region with that of the right electrode, between which the electron transmission from the $B_σ$ band of the right electrode to that of the left electrode is allowable and the probability is close to 1. Fig. 3(b) and (c) show the electron transmission eigenstates and pathway at the E_F under the bias of 0.3 V, respectively. It can be seen that the electron transmission channel is mainly distributed at the bare B edge (shown in Fig. 3(b)), and the local current (from the left to the right) belongs to the B→B hop current (shown in Fig. 3(c)). The energy overlapping region is larger than that of the bias window region at 0.3 V, but it gets smaller when the bias goes beyond 0.3 V and thus results in narrower transmission peak within the bias window. Therefore, a current peak appears at 0.3 V, and the NDR phenomenon is presented subsequently. For instance, when the bias increases up to 0.8 V, the $B_σ$ band of left electrode has no overlaps with that of the right electrode. Thus, the electron transmission between them is forbidden, leading to zero transmission coefficients near the E_F. Now then,

the current decreases to zero at this threshold voltage (about 0.8 V).
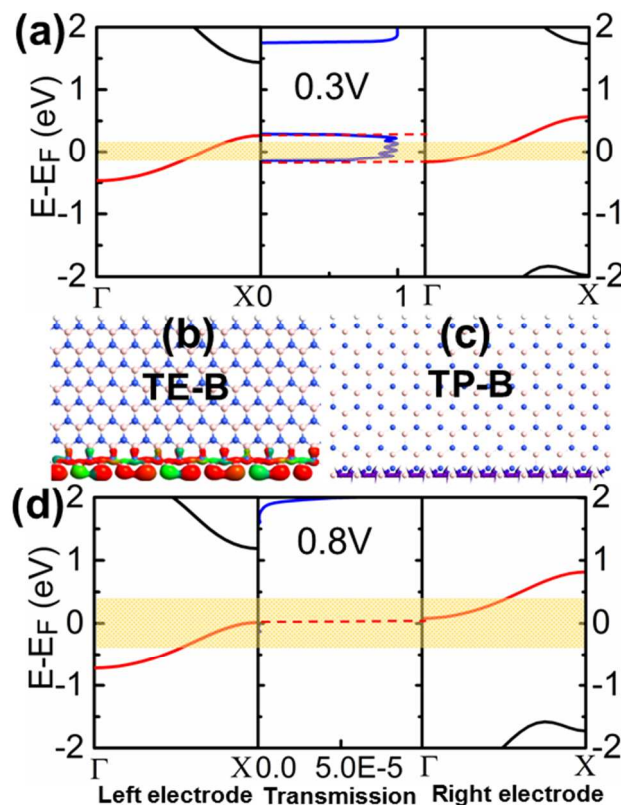
Fig. 3 Band structure for the left electrode, transmission spectrum, and band structure for the right electrode under 0.3 V (a) and 0.8 V (d) biases for 8BNNR-NH, and the transmission eigenstates (b) and pathway (c) at the Fermi level under the bias of 0.3 V. The Fermi level is set at zero. The red dotted lines refer to the overlapping region between the bands of the left and right electrodes. The yellow shadows denote the bias window.

Fig. 4(a) and (b) display the bias-dependent transmission spectra and band structures of both left and right electrodes for the 8-ZBNNR-BH. The band of the left electrode has large overlaps with that of the right electrode, especially in the negative energy region. Thus, the electron transmission between them is favorable. For instance, at the bias of 0.2 V, the transmission coefficient at –0.1 eV (chemical potential of the left electrode) is close to 2. Now, there are two transmission channels in the electron propagating through the nanoribbons, i.e., TE-N1 (contributed by the $N_π$ bands of the right and left electrodes), and TE-N2 (contributed by the $N_σ$ bands of the two electrodes), respectively, as shown in the right side of Fig. 4(a). The transmission pathway (labeled as TP-N) indicates that the local currents mainly propagates along three channels, i.e., N→B bond current, as well as N→N and N→B hop current channels. When the bias goes beyond 0.2 V, the $N_σ$ and $N_π$ bands of the left electrode shift away from the Fermi level, and they almost keep the same overlaps with that of the right electrode within the bias window. As a result, the transmission coefficient decreases slightly, and then the current through 8-ZBNNR-BH slightly declines (i.e., NDR behavior). While, when the bias reaches up to 0.8 V, only the $N_π$ band of the left electrode still overlaps with that of the right electrode within

the bias window. Now, there is only one transmission channel, i.e., TE-N1' (at −0.4 eV), which is contributed by the N_π bands of the two electrodes. The local current mainly belongs to the N→B bond current according to the transmission pathway TP-N'. Therefore, unlike the case of 8-ZBNNR-NH, the current through 8-ZBNNR-BH at a high bias (greater than 0.8 V) only decreases to any non-zero steady value.
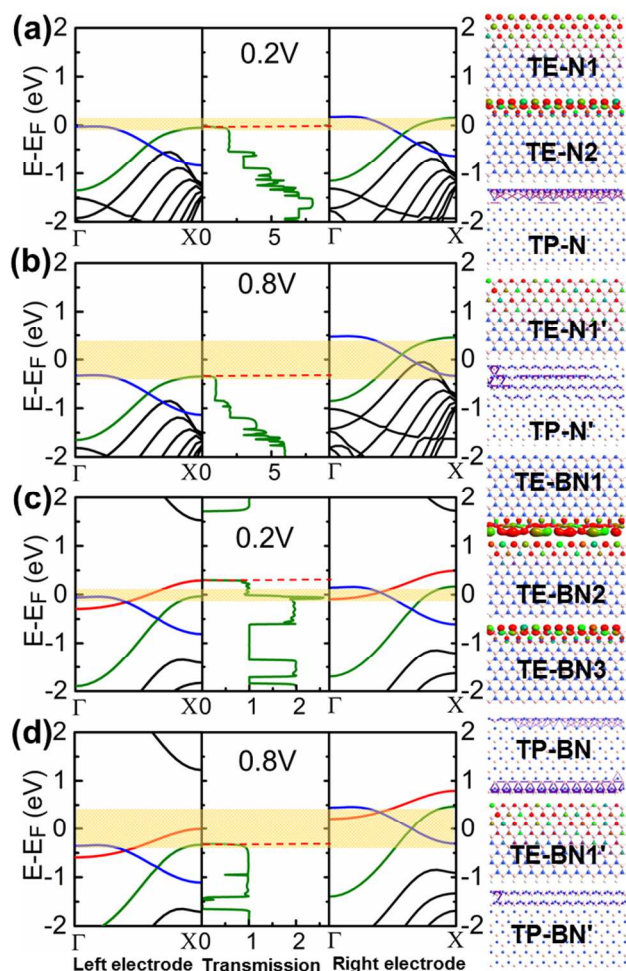
Fig. 4 Band structures of the left and right electrodes, transmission spectrum, and transmission eigenstates under 0.2 V and 0.8 V bias, respectively. (a) and (b) for 8-ZBNNR-BH, (c) and (d) for 8-ZBNNR. The Fermi level is set at zero. The transmission eigenstates and pathways are plotted in the right side.

The NDR mechanisms of 8-ZBNNR-NH and 8-ZBNNR-BH also apply for the case of the 8-ZBNNR device. It is worth noting that, at the bias of 0.2 V (namely, at the current peak shown in Fig. 1(b)), there are three transmission channels at −0.06 eV, i.e., TE-BN1 (contributed by the B_σ bands of the two electrodes), TE-BN2 (contributed by the N_π bands of the two electrodes), and TE-BN3 (contributed by the N_σ bands of the two electrodes), respectively. According to the corresponding transmission pathway at −0.06 eV, it is found that there are four local current channels, i.e., three N→N, N→B, and B→B hop current channels, as well as one N→B bond current channel. Nevertheless, each of the three bands (i.e., B_σ, N_σ, and N_π) of the left electrode overlaps with that of the right electrode, as shown in Fig. 4(c). Within the bias window, the transmission coefficient is large and even close to 3 at −0.06 eV. Thus, the

current peak appears at the bias of 0.2 V, which is larger than that of 8-ZBNNR-NH and 8-ZBNNR-BH devices. While, with the bias increasing, both N_σ and N_π shift away from the E_F level, even the overlaps of the B_σ and N_σ bands for both the left and right electrodes become smaller until they disappear successively. For instance, at the bias of 0.8 V shown in Fig. 4(d), only N_π bands of the two electrodes overlap within the bias window. One transmission channel TE-BN1' (at −0.4 eV, contributed by the N_π bands of the two electrodes) is available, and the corresponding transmission pathway indicates the local current belongs to the N→B bond current. As a result, the transmission coefficients within the bias window decrease gradually, leading to the decreased current to any non-zero steady value at last, like the case of the 8-ZBNNR-BH, as shown in Fig. 1(b).
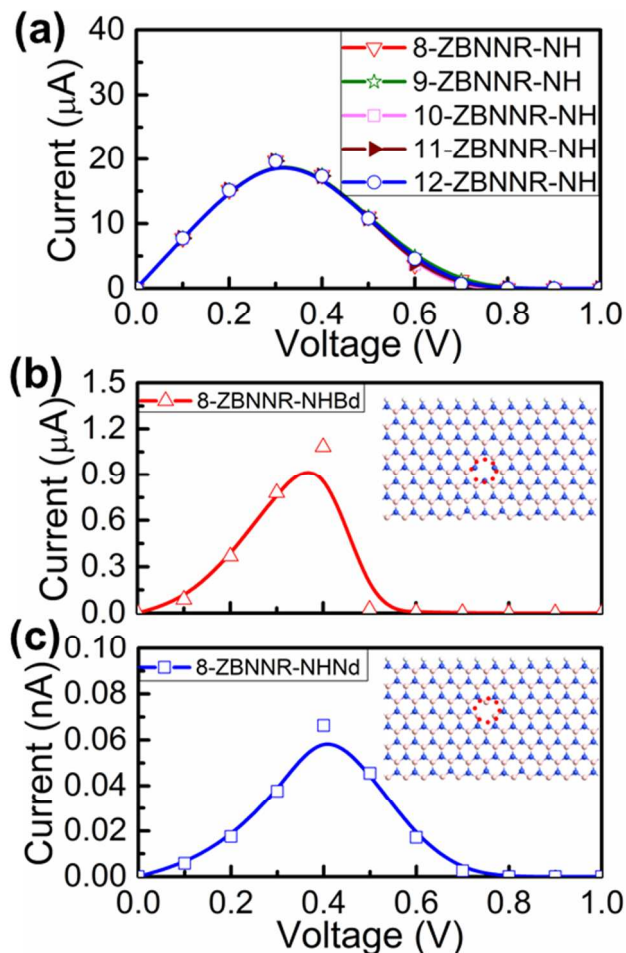
Fig. 5 (a) The *I–V* curves of ZBNNR-NH with different widths. The *I–V* curves of 8-ZBNNR-NH device with a B (b) and N (c) atom vacancy defect. The inset in (b) and (c) refers to the scattering region of the device, respectively.

To further understand the effect of ribbon widths on the charge transport properties of ZBNNRs, the ribbon width is gradually increased. The *I–V* curves of four ZBNNRs-NH with a larger ribbon width (namely, 9-ZBNNR-NH, 10-ZBNNR-NH, 11-ZBNNR-NH, and 12-ZBNNR-NH) were further explored and plotted in Fig. 5(a), from which we can see that these four ZBNNRs-NH with a larger width present the same charge transport properties compared to the case of the 8-ZBNNR-NH. This is mainly ascribed to that they have the very

similar band structures around the E_F level and thus the same NDR mechanism simultaneously. The same charge transport properties were also found for the cases of ZBNNR-BH and ZBNNR with a larger ribbon width. Unlike the ZGNRs, the ZGNRs with *odd*-numbered chains present entirely different charge transport properties from that with *even*-numbered chains in spite of their similar band structures.[38] It reveals that under the finite biases the charge transport properties of perfect ZBNNRs with one or two bare edges do not show obvious dependencies on their widths. The NDR is one intrinsic characteristic of the perfect zigzag boron nitride nanoribbons, which is different from that it can be obtained in graphene nanoribbons by defecting,[9] doping,[32] etc.

In addition, defects (such as vacancies) are generally unavoidable during the growth process of a sample.[13] Whether a vacancy defect affects the intrinsic NDR characteristics of ZBNNRs is unknown. Here, two models are considered, i.e., 8-ZBNNR-NH with a boron atom vacancy defect (labeled as 8-ZBNNR-NHBd) and with a nitrogen atom vacancy defect (labeled as 8-ZBNNR-NHNd) in the central scattering region, as shown in the insets of Fig. 5(b) and (c). Their *I–V* curves are depicted in Fig. 5(b) and (c). We can see that the NDR behaviors still survive in the two defective structures. The only difference is that their current amplitudes decrease by several orders of magnitude. This is due to the fact that the vacancy defect breaks the edge states and produces some localized defect-induced states, which suppress the electron transmission and diminish the current. Therefore, some ZBNNR-based nanoscale NDR devices owning different current peaks and peak to valley ratios with various orders of magnitude are promising candidates in devices, such as digital applications,[39,40] amplification,[41] and oscillators,[42] etc. What's more, the BCN nanoribbons also depict the NDR behaviors,[22] which demonstrates that the intrinsic NDR characteristics of ZBNNRs are preserved in spite of the carbon-doping.

4 Conclusions

In conclusion, using the first-principles density functional theory combined with non-equilibrium Green's function method, we investigate the charge transport properties of ZBNNRs with various hydrogen passivations. The results show that these ZBNNR-based devices present the NDR characteristics except the models whose both edges are passivated, due to the mechanism that the overlaps of the bands near the Fermi level between the left and right electrodes get smaller or even disappear under the high biases. The charge transport properties of the perfect ZBNNRs with one or two bare edges do not show obvious dependencies on their widths. The electrons propagating through the ZBNNR-NH devices mainly occurs at the bare B edge, via the B→B hop current channel. While, there exist the N→B bond current, B→N and N→N hop current (under a low bias) in the ZBNNR-BH devices at the bare N edge. For the ZBNNRs without hydrogen passivations, there exist the similar current channels like that of the ZBNNR-BH devices, except one additional B→B hop current channel (under a low bias). The NDR is the intrinsic characteristic of the ZBNNR-based devices, including some defective structures, i.e., with a boron or nitrogen atom vacancy defect. The results demonstrate that the ZBNNR-based nanostructures have the potential applications in the nanoscale electronics, i.e., as the candidate materials for the NDR devices.

Notes and references

a College of Physics and Electronic engineering, Henan Normal University, Xinxiang 453007, China.
Correspondence to ypan@htu.edu.cn.
b School of Physics and Optoelectronic Engineering, Ludong University, Yantai 264025,China

1 K. S. Novoselov, D. Jiang, F. Schedin, T. J. Booth, V. V. Khotkevich, S. V. Morozov and A. K. Geim, *Proc. Natl. Acad. Sci. U.S.A.*, 2005, **102**, 10451−10453.

2 K. S. Novoselov, A. K. Geim, S. V. Morozov, D. Jiang, Y. Zhang, S. V. Dubonos, I. V. Grigorieva and A. A. Firsov, *Science*, 2004, **306**, 666−669.

3 K. S. Novoselov, A. K. Geim, S. V. Morozov, D. Jiang, M. I. Katsnelson, I. V. Grigorieva, S. V. Dubonos and A. A. Firsov, *Nature*, 2005, **438**, 197−200.

4 C. W. J. Beenakker, *Rev. Mod. Phys.*, 2008, **80**, 1337−1354.

5 A. H. Castro Neto, F. Guinea, N. M. R. Peres, K. S. Novoselov and A. K. Geim, *Rev. Mod. Phys.*, 2009, **81**, 109−162.

6 S. D. Sarma, S. Adam, E. H. Hwang and E. Rossi, *Rev. Mod. Phys.*, 2011, **83**, 407−470.

7 F. Tseng, D. Unluer, K. Holcomb, M. R. Stan and A. W. Ghosh, *Appl. Phys. Lett.*, 2009, **94**, 223112.

8 H. Ren, Q. X. Li, Y. Luo and J. L. Yang, *Appl. Phys. Lett.*, 2009, **94**, 173110.

9 Y. P. An and Z. Q. Yang, *Appl. Phys. Lett.*, 2011, **99**, 192102.

10 K. M. Milaninia, M. A. Baldo, A. Reina and J. Kong, *Appl. Phys. Lett.*, 2010, **95**, 183105.

11 D. B. Farmer, Y. M. Lin and P. Avouris, *Appl. Phys. Lett.*, 2010, **97**, 013103.

12 M. Terrones, J. -C. Charller, A. Gloter, E. Cruz-Silva, E. Terrés, Y. B. Li, A. Vinu, Z. Zanolli, J. M. Dominguez, H. Terrones, Y. Bando and D. Golberg, *Nano Lett.*, 2008, **8**, 1026−1032.

13 N. Alem, R. Erni, C. Kisielowski, M. D. Rossell, W. Gannett and A. Zettl, *Phys. Rev. B*, 2009, **80**, 155425.

14 Y. Liao, Z. Chen, J. W. Connell, C.C. Fay, C. Park, J. W. Kim and Y. Lin, *Adv. Funct. Mater.* 2014, **24**, 4497−4506.

15 H. B. Zeng, C. Y. Zhi, Z. H. Zhang, X. L. Wei, X. B. Wang, W. L. Guo, Y. Bando and D. Goberg, *Nano Lett.*, 2008, **10**, 5049−5055.

16 X. B. Wang, Q. Weng, X. Wang, X. Li, J. Zhang, F. Liu, X. F. Jiang, H. Guo, N. Xu, D. Golberg and Y. Bando, *ACS Nano*, 2014, DOI: 10.1021/nn502486x.

17 F. Liu, X. Mo, H. Gan, T. Guo, X. Wang, B. Chen, J. Chen, S. Deng, N. Xu, T. Sekiguch, D. Golberg and Y. Bando, *Sci. Rep.*, 2014, **4**, 4211.

18 F. W. Zheng, G. Zhou, Z. R. Liu, J. Wu, W. H. Duan, B. L. Gu and S. B. Zhang, *Phys. Rev. B*, 2008, **78**, 205415.

19　F. L. Zheng, Y. Zhang, J. M. Zhang and K. W. Xu, *J. Phys. Chem. Solids*, 2011, **72**, 256.

20　Y. Pan and Z. Q. Yang, *Phys. Rev. B*, 2010, **82**, 195308.

21　W. Chen, Y. Li, G. Yu, Z. Zhou and Z. Chen, *J. Chem. Theory. Comput.*, 2009, **5**, 3088−3095.

22　Y. Zhou, J. Zhang, C. Ye, X. Miao and D. Zhang, *J. Appl. Phys.*, 2014, **115**, 114313.

23　V. Barone and J. E. Peralt, *Nano Lett.*, 2008, **8**, 2210−2214.

24　Q. Tang, Z. Zhou, P. Shen and Z. Chen, *Chem. Phys. Chem.*, 2013, **14**, 1787.

25　Q. Tang, J. Bao, Y. Li, Z. Zhou and Z. Chen, *Nanoscale*, 2014, **6**, 8624−8634.

26　Z. Zhang, W. Guo and B. I. Yakobson, *Nanoscale*, 2013, **5**, 6381−6387.

27　W. Chen, Y. Li, G. Yu, C. Z. Li, S. B. Zhang, Z. Zhou and Z. Chen, *J. Am. Chem. Soc.*, 2010, **132**, 1699−1705.

28　Q. Tang, Z. Zhou and Z. Chen, *J. Phys. Chem. C*, 2011, **115**, 18531−18537.

29　Y. Lin and J. W. Connell, *Nanoscale*, 2012, **4**, 6908−6939.

30　D. H. Kim, W. T. Kim, E. S. Park, N. Mattern and J. Eckert, *Prog. Mater. Sci.*, 2013, **58**, 1103−1172.

31　K. S. Kim, C. T. Kingston, A. Hrdina, M. B. Jakubinek, J. Guan, M. Plunkett and B. Simard, *ACS Nano*, 2014, **8**, 6211−6220.

32　H. Ren, Q. X. Li, Y. Luo and J. L. Yang, *Appl. Phys. Lett.*, 2009, **94**, 173110.

33　M. Brandbyge, J. L. Mozos, P. Ordejón, J. Taylor and K. Stokbro, *Phys. Rev. B*, 2002, **65**, 165401.

34　J. Taylor, H. Guo and J. Wang, *Phys. Rev. B*, 2001, **63**, 121104.

35　J. M. Soler, E. Artacho, J. D. Gale, A. García, J. Junquera, P. Ordejón and D. Sánchez-Portal, *J. Phys.: Condens. Matter*, 2002, **14**, 2745−2779.

36　N. Troullier and J. L. Martins, *Phys. Rev. B*, 1991, **43**, 1993−2006.

37　M. Büttiker, Y. Imry, R. Landauer and S. Pinhas, *Phys. Rev. B*, 1985, **31**, 6207−6215.

38　Z. Y. Li, H. Y. Qian, J. Wu, B. L. Gu and W. H. Duan, *Phys. Rev. B*, 2008, **100**, 206802.

39　T. P.E. Broekaert, B. Brar, J. P. A. vanderWagt, A. C. Seabaugh, F. J. Morris, T. S. Moise, E. A. Beam and G. A. Frazir, *IEEE J. Solid-State Circuits*, 1998, **33**, 1342−1349.

40　R. H. Mathews, J. P. Sage, T. C. L. G. Sollner, S. D. Calawa, C. L. Chen, L. J. Mahoney, P. A. Maki and K. M. Movlvar, *Proc IEEE*, 1999, **87**, 596−605.

41　A. L. McWhorter and A. G. Foyt, *Appl. Phys. Lett.*, 1966, **9**, 300.

42　E. R. Brown, J. R. Söderström, C. D. Parker, L. J. Mahoney and K. M. Molvar, *Appl. Phys. Lett.*, 1991, **58**, 2291.